

# High resonance frequency force microscope scanner using inertia balance support

メタデータ	言語: English 出版者: 公開日: 2017-10-06 キーワード: 作成者: Fukuma, Takeshi, Okazaki, Yasutaka, Kodera, Noriyuki, Uchihashi, Takayuki, Ando, Toshio, 福間, 剛士, 古寺, 哲幸, 内橋, 貴之, 安藤, 敏夫 メールアドレス: 所属:
URL	<a href="https://doi.org/10.24517/00039986">https://doi.org/10.24517/00039986</a>

This work is licensed under a Creative Commons Attribution-NonCommercial-ShareAlike 3.0 International License.



## High resonance frequency force microscope scanner using inertia balance support

Takeshi Fukuma,<sup>1(a)</sup> Yasutaka Okazaki,<sup>2</sup> Noriyuki Kodera,<sup>2</sup> Takayuki Uchihashi,<sup>2</sup> and Toshio Ando<sup>2</sup>

<sup>1</sup>Frontier Science Organization, Kanazawa University, Kakuma-machi, 920-1192 Kanazawa, Japan and PRESTO, Japan Science and Technology Agency, 4-1-9 Honcho Kawaguchi, Saitama, Japan

<sup>2</sup>Physics Department, Kanazawa University, Kakuma-machi, 920-1192 Kanazawa, Japan

(Received 3 May 2008; accepted 5 June 2008; published online 19 June 2008)

We have developed the atomic force microscope scanner with the high resonance frequency of 540 kHz in the  $z$  axis using a piezosupport mechanism “inertia balance support.” In the method, a cubic piezoactuator is supported at the four sides perpendicular to the extension axis, by which the resonance frequency of the scanner remains as high as that of the actuator in the free vibration. The scanner allows driving at low voltage  $\pm 15$  V for the practical  $z$  scan range of 330 nm. We demonstrate the applicability of the scanner to the true-atomic-resolution imaging of mica in liquid. © 2008 American Institute of Physics. [DOI: 10.1063/1.2951594]

The improvement of the imaging speed in atomic force microscopy<sup>1</sup> (AFM) has great advantages in the practical applications. The higher imaging speed gives the higher throughput in defect testing of semiconductor devices, which is one of the biggest industrial applications of AFM. For biological applications, high-speed imaging enables visualizing dynamic behavior of proteins in physiological environments.<sup>2,3</sup>

The resonance frequency of the AFM scanner, especially in the  $z$  direction ( $f_z$ ), is the major factor that limits the imaging speed in AFM. A piezotube scanner is the most widely used but has a relatively low  $f_z$  (typically  $< 1$  kHz). Efforts have been made for enhancing  $f_z$  by employing shear piezoactuators,<sup>4</sup> counter balance,<sup>2</sup> flexural support,<sup>5,6</sup> etc. Among the most sophisticated design was reported by Ando *et al.* in 2001.<sup>2</sup> The scanner has a high  $f_z$  of 180 kHz and has been used for visualizing biological processes at video rate.<sup>2,3</sup>

In this letter, we propose a design of the high-speed AFM scanner using the “inertia balance support” mechanism. The distinctive features of the developed scanner include high  $f_z$  of 540 kHz, simple structure and compact size ( $7 \times 7 \times 3$  mm<sup>3</sup>), applicability to the atomic-resolution imaging, and compatibility with low-voltage drive ( $\pm 15$  V for  $z$  scan range of 330 nm). The low-voltage drive eliminates the risk of electrocution in liquid environment applications. In addition, a low voltage buffer amplifier has a much higher bandwidth and a better noise figure than a high-voltage amplifier, making it ideal for the high-speed and high-resolution imaging in liquid. Here we show the detailed design and performance of the developed scanner with demonstration of the true atomic resolution by imaging mica in liquid.

In a typical design for the  $z$  scanner, one end of a piezoactuator with a resonance frequency of  $f_0$  is fixed on a metal plate and the other end is free to move. This fixation gives rise to another vibration mode at the frequency  $f_0/2$ , leading to a lower  $f_z$  value. In addition, the whole actuator moves toward the free end upon application of a driving voltage so that the center of mass is also displaced in the same direction

to produce an impulsive force. The impulsive force is transmitted to the other mechanical components such as  $x$  and  $y$  scanners and excites the vibrations at low resonance frequencies. Such vibrations could produce a displacement in the  $z$  direction or could be transmitted back to the  $z$  scanner. Consequently,  $f_z$  is limited to values much lower than  $f_0$ .

In order to solve this problem, we have employed the inertia balance support mechanism for the fixation of a piezoactuator. Figures 1(a) and 1(b) show the schematic model and the photograph of the developed AFM scanner. In this design, the  $z$  scanner consists of  $2 \times 2 \times 2$  mm<sup>3</sup> monolithic piezoactuator placed inside a hole at the center of the support. The diameter of the hole is approximately 30  $\mu$ m shorter than the diagonal of the cross section of the actuator so that the actuator is supported by the lateral force applied to the four sides perpendicular to the  $z$  axis. In this configuration, the actuator equally extends in both sides of the  $z$  axis. Thus,  $f_z$  remains as high as  $f_0$ . Moreover, the scanner motion hardly displaces the center of mass and hence the impulsive force generated by the actuator is much smaller than that in the typical fixation at one end.

Figures 2(a) and 2(b) respectively show the amplitude and phase of the  $z$  vibration induced by driving the  $z$  scanner. The  $z$  vibration was measured with a cantilever in contact with the  $z$  scanner. The curve shows a clean single peak at 540 kHz, which approximately agrees with the resonance

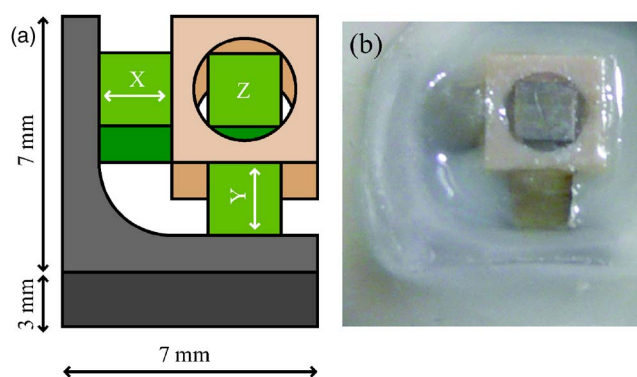


FIG. 1. (Color online) (a) Schematic model and (a) the photograph of the developed scanner. The scanner has the dimension of  $7 \times 7 \times 3$  mm<sup>3</sup>.

<sup>a</sup>Electronic mail: fukuma@staff.kanazawa-u.ac.jp.

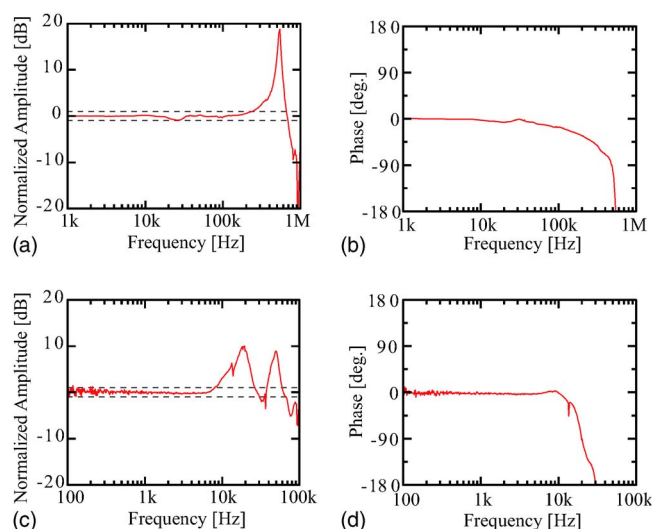


FIG. 2. (Color online) (a) Amplitude and (b) phase of the  $z$  vibration induced by driving the  $z$  scanner. (c) Amplitude and (d) phase of the  $z$  vibration induced by driving the  $x$  scanner. The characteristics for the  $y$  scanner is approximately the same as that for the  $x$  scanner. The  $z$  vibration was measured from the deflection of a cantilever (NCH: Nanosensors) in contact with the  $z$  scanner. The amplitude is normalized at the low frequency values. The dotted lines in (a) and (c) corresponds to the values of  $\pm 1$  dB.

frequency of the piezoactuator in the free vibration (510–550 kHz). This demonstrates that the inertia balance support can prevent the reduction of  $f_z$  due to the fixation. The amplitude and phase responses show typical profiles for a second order vibration system so that they can be easily reproduced with a simple  $LCR$  circuit. Thus, it is not difficult to suppress the resonance peak at 540 kHz using the active  $Q$  control method<sup>7</sup> for further extending the effective  $f_z$  value.

The piezoactuators for the  $x$  and  $y$  axes are fixed on the side of the  $z$  scanner as shown in Fig. 1. This configuration is essentially the same as that in the tripod scanner.<sup>8</sup> Namely, the displacement of the  $x$  and  $y$  actuators induce the displacement of the  $z$  scanner as well as the distortion in the whole scanner. Due to the small displacement (nanometer range) compared to the scale of the scanner (millimeter range), the displacement of the  $z$  scanner caused by the distortion is negligible.

This structure allows designing the scanner to be simple and compact, as shown in Fig. 1(a). Since the  $x$  and  $y$  scanners are not placed either over or under the  $z$  scanner, the mechanical coupling between the  $x$ ,  $y$  scanners and the  $z$  scanner remains relatively small. In addition, the free space under the  $z$  scanner makes it possible to add a counterbalance for compensating the possible weight increase on the upper side of the  $z$  scanner.

The free space in the scanner is filled with elastomer having a high loss factor to absorb the energy of the spurious mechanical vibrations [Fig. 1(b)]. This also helps to mechanically isolate the  $z$  scanner from the other mechanical components.

In Figs. 2(a) and 2(b), there are small peaks at 20–30 kHz. These minor peaks are caused by the coupling between the  $z$  scanner and other mechanical components. However, the magnitude of the amplitude peak is less than 1 dB as indicated by the dotted lines in Fig. 2(a). The magnitude of the phase peak is as small as the slight phase delay of the  $z$  actuator itself. Therefore, these minor peaks are unlikely to cause problems in a practical application.

Figures 2(c) and 2(d) show the amplitude and phase of the  $z$  vibration induced by driving the  $x$  scanner. The  $z$  vibration was measured from the deflection of the cantilever in contact with the  $z$  scanner. Although these curves do not show the pure characteristics of the  $x$  scanner itself, they practically determine the maximum driving frequency for the  $x$  scanner. The  $y$  scanner shows similar characteristics to those of the  $x$  scanner.

Figure 2(c) shows that the gain variation is kept less than  $\pm 1$  dB up to 8 kHz. For obtaining a  $256 \times 256$  pixel image at 30 frame/s, the required driving frequency of the  $x$  scanner is 7.7 kHz. Thus, the maximum  $x$  driving frequency of 8 kHz is high enough even for the video-frame imaging.

The piezoactuators used for the  $x$ ,  $y$ , and  $z$  scanners have the driving voltage range from  $-20$  to  $100$  V, which corresponds to the displacement range from  $-440$  nm to  $2.2 \mu\text{m}$  ( $22$  nm/V). Since the  $z$  actuator equally extends to the both sides of the  $z$  axis, the displacement becomes half of the whole extension ( $11$  nm/V). For the low drive voltage  $\pm 15$  V, the scan range is  $660$  nm in  $xy$  and  $330$  nm in  $z$ . This scan range is large enough for most of the high-resolution imaging applications.

We have integrated the developed scanner into a home-built frequency modulation AFM (FM-AFM) with a low noise cantilever deflection sensor.<sup>9,10</sup> The deflection noise density of the sensor is less than  $10 \text{ fm}/\sqrt{\text{Hz}}$ ,<sup>10</sup> which is essential for oscillating a stiff cantilever with small amplitude ( $<0.5$  nm) and thereby obtaining the true atomic resolution.<sup>11</sup>

The scanner was driven with a home-built buffer amplifier with an output range of  $\pm 15$  V. The root-mean-square (rms) output noise of the driver is about  $35 \text{ nV}/\sqrt{\text{Hz}}$ , which corresponds to the  $z$  displacement noise of  $0.27$  pm for a bandwidth of  $500$  kHz and the piezosensitivity of  $11$  nm/V. In order to obtain clear true atomic-resolution images, the  $z$  displacement noise level in the feedback condition should be less than  $10$  pm. Thus, the instrumentation noise is required to be less than  $1$  pm. The combination of the developed scanner and the low voltage buffer amplifier can satisfy these stringent requirements even for a wide bandwidth of  $500$  kHz.

For the purpose of comparison, we also measured the output noise of a commercially available high-voltage amplifier (ENP-4014B: Echo Electronics). We confirmed that the amplifier is applicable to the true atomic resolution imaging at a relatively low imaging speed ( $<1$  frame/min) with a piezotube scanner. The output noise density was  $2 \mu\text{V}/\sqrt{\text{Hz}}$  for the gain from  $0$  to  $26$  dB. The corresponding  $z$  noise level for  $500$  kHz bandwidth is  $15$  pm. This could prevent the atomic-resolution imaging at a high imaging rate.

Figure 3(a) shows an FM-AFM image taken in phosphate buffer solution using the developed scanner driven with the home-built low voltage buffer amplifier. The image shows the honeycomblike structure which is characteristic of the cleaved mica surface [Fig. 3(b)]. The individual atoms constituting the honeycomb lattice are resolved in the image, which demonstrates that the developed scanner is applicable to the atomic-resolution imaging.

The tip was scanned at the velocity of  $732$  nm/s, which is relatively fast for the atomic-resolution imaging. For example, obtaining a  $128 \times 64$  pixel image on  $5 \times 2.5 \text{ nm}^2$  area with this tip velocity takes  $0.87$  s. The present imaging speed

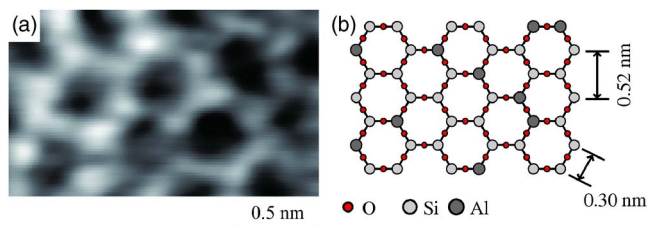


FIG. 3. (Color online) (a) FM-AFM image of mica in phosphate buffer solution.  $2 \times 1.2 \text{ nm}^2$ ,  $\Delta f = -50 \text{ Hz}$ , tip velocity:  $732 \text{ nm/s}$ . A Si cantilever (NCH: Nanosensors) with a resonance frequency of about  $130 \text{ kHz}$  and  $Q$  factor of 8 in liquid was used. The scanner was driven with a low voltage buffer amplifier ( $\pm 15 \text{ V}$ ). (b) Schematic model of the cleaved mica surface.

of our AFM is no longer limited by the resonance frequency of the  $z$  scanner but by the bandwidth of the FM detector ( $\sim 1.2 \text{ kHz}$ ). The high signal-to-noise ratio of the image shown in Fig. 3(a) suggests that the imaging speed is not limited by the force sensitivity at the feedback bandwidth. Therefore, further improvement of the imaging speed should be possible by enhancing the bandwidth of the FM detector.

In this study, we developed the high-speed AFM scanner with the high resonance frequency of  $540 \text{ kHz}$ . We also applied the developed scanner to the atomic-resolution imaging by FM-AFM in liquid. For developing a high-speed and high-resolution AFM, all the components involved in the main tip-sample distance feedback loop must be optimized

by enhancing the bandwidth and reducing the noise level. We presented the way to enhance the scanner bandwidth using the inertia balance support and to reduce the  $z$  displacement noise using the low-voltage buffer amplifier.

This research was supported by PREST, Japan Science and Technology Agency.

- <sup>1</sup>G. Binnig, C. F. Quate, and C. Gerber, *Phys. Rev. Lett.* **56**, 930 (1986).
- <sup>2</sup>T. Ando, N. Kodera, E. Takai, D. Maruyama, K. Saito, and A. Toda, *Proc. Natl. Acad. Sci. U.S.A.* **98**, 12468 (2001).
- <sup>3</sup>T. Ando, T. Uchihashi, N. Kodera, A. Miyagi, R. Nakakita, H. Yamashita, and M. Sakashita, *Jpn. J. Appl. Phys., Part 1* **45**, 1897 (2006).
- <sup>4</sup>M. J. Rost, L. Crama, P. Schakel, E. van Tol, G. B. E. M. van Velzen-Williams, C. F. Overgaw, H. ter Horst, H. Dekker, B. Okhuijsen, M. Seynen, A. Vijftigschild, P. Han, A. J. Katan, K. Schoots, R. Schumm, W. van Loo, T. H. Oosterkamp, and J. W. M. Frenken, *Rev. Sci. Instrum.* **76**, 053710 (2005).
- <sup>5</sup>J. H. Kindt, G. E. Fantner, J. A. Cutroni, and P. K. Hansma, *Ultramicroscopy* **100**, 259 (2004).
- <sup>6</sup>T. Ando, N. Kodera, T. Uchihashi, A. Miyagi, R. Nakakita, H. Yamashita, and K. Matada, *e-J. Surf. Sci. Nanotechnol.* **3**, 384 (2005).
- <sup>7</sup>N. Kodera, H. Yamashita, and T. Ando, *Rev. Sci. Instrum.* **76**, 053708 (2005).
- <sup>8</sup>G. Binnig, H. Rohrer, C. Gerber, and E. Weibel, *Phys. Rev. Lett.* **49**, 57 (1982).
- <sup>9</sup>T. Fukuma, M. Kimura, K. Kobayashi, K. Matsushige, and H. Yamada, *Rev. Sci. Instrum.* **76**, 053704 (2005).
- <sup>10</sup>T. Fukuma and S. P. Jarvis, *Rev. Sci. Instrum.* **77**, 043701 (2006).
- <sup>11</sup>T. Fukuma, K. Kobayashi, K. Matsushige, and H. Yamada, *Appl. Phys. Lett.* **87**, 034101 (2005).